Intermediate-Mass Fragment Decay of the Neck Zone Formed in Peripheral ^{209}Bi $+^{136}$ Xe Collisions at $E_{lab}/A = 28$ MeV

J. Tõke, B. Lott,* S. P. Baldwin, B. M. Quednau,† and W. U. Schröder
Department of Chemistry and Nuclear Structure Research Laboratory, University of Rochester, Rochester, New York 14627

L. G. Sobotka, J. Barreto,‡ R. J. Charity, D. G. Sarantites, and D. W. Stracener§
Department of Chemistry, Washington University, St. Louis, Missouri 63130

R. T. de Souza
Department of Chemistry and Indiana University Cyclotron Facility, Indiana University, Bloomington, Indiana 47405
(Received 16 June 1995)

Intermediate-mass fragments (IMF) from the ^{209}Bi+^{136}Xe reaction at $E_{lab}/A = 28$ MeV have been measured in coincidence with other reaction products, using a highly efficient 4π detector setup. Their emission patterns exhibit features consistent with dynamical fragmentation of a neck zone between the reaction partners, in addition to sequential statistical emission. In peripheral collisions with an average of 0.3 GeV of dissipated kinetic energy, the dynamical process accounts for 0.24 of the observed IMF multiplicity of 0.33.

PACS numbers: 25.70.Pq, 25.70.Lm

In recent years, studies of heavy-ion reactions at bombarding energies per nucleon comparable to nucleonic Fermi energies have focused on the production of intermediate-mass fragments (IMF) [1–4]. The fact that multiplicities of IMF's released in such collisions are often noticeably higher than predicted by standard statistical-model calculations for the decay of hot, but otherwise "normal," nuclear systems, has prompted modeling of various scenarios favoring copious production of IMF's. The considered scenarios for efficient IMF production mostly involve bulk instabilities of nuclear matter, driven to unusual thermodynamical states in the course of near-central collisions. This kind of instability is thought to arise, for example, as a result of a phase transition induced by the isentropic expansion of a hot nuclear system [5,6]. Many important features of IMF production have been reported to find a qualitative, or even quantitative, explanation within the framework of this type of model. At the same time, experimental evidence has mounted for alternative, efficient IMF production mechanisms that do not involve the bulk system [7,8] and that are more of a dynamical than a statistical character. A notable example of such a mechanism is that of multiple neck rupture, which has been considered in low-energy fission and heavy-ion studies [9–12]. A similar process has been observed in heavy-ion [13–17] or light-ion [18] induced ternary fission and in simulations involving collisions of macroscopic droplets [19,20]. Also, theoretical models have been advanced in the past to describe instabilities which may possibly lead to IMF release [21]. The present work demonstrates that phenomena involving local, dynamically driven instabilities play a significant role also in heavy-ion reactions at intermediate bombarding energies. Apart from its value for the general understanding of the intermediate-energy heavy-ion collision dynamics, the type of dynamical IMF production encountered in the present system and in the lighter system of ^{nat}Cu+^{129}Xe at $E/A = 50$ MeV [22], may offer a unique tool of probing specifically the fast approach and reseparation stages of peripheral collisions.

The present analysis focuses on peripheral collisions, where the dynamical IMF production mechanism is most clearly seen and was actually first noticed [23–25]. Such collisions are characterized by low excitation energies and follow mostly well-defined binary reaction scenarios [26–28], both features facilitating the analysis of the IMF yield distribution.

The experiment was performed at the National Superconducting Cyclotron Laboratory of Michigan State University. A beam of 28-MeV/nucleon ^{136}Xe ions from the K1200 cyclotron was focused on a self-supporting 1.5-mg/cm^2 ^{209}Bi target, surrounded by a detector setup which provided close to 4π angular coverage for neutrons, light charged particles (LCP), and IMF's. Neutrons were detected using the Rochester RedBall neutron multiplicity meter (NMM), operated in a geometrical configuration and with electronic settings ensuring a detection efficiency of about 70% for neutrons emitted from slow-moving sources. LCP's and IMF's were detected using the Washington University Dwarf Array [29], configured with 95 plastic-CsI phoswich detectors to cover about 90% of 4π. This array provided atomic-number identification for $Z = 1$ to $Z = 14–25$ (depending on the detector), with an energy threshold of approximately 4 MeV/nucleon. Additionally, in order to detect massive products, three multielement, position-sensitive silicon detectors were placed at forward angles. Only the most forward of these telescopes, covering an angular

 0031-9007/95/75(16)/2920(4)$06.00

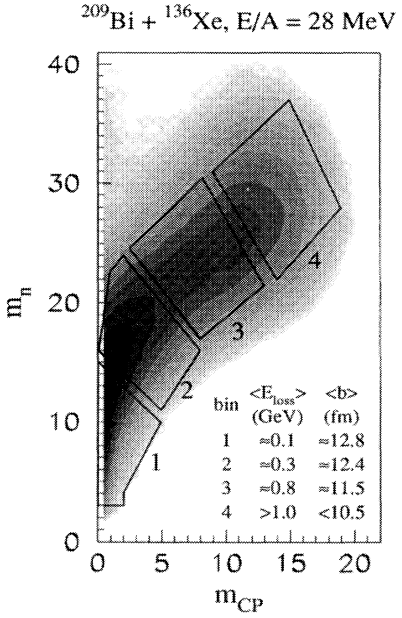

FIG. 1. Logarithmic contour plot of the joint distribution of neutron and charged-particle multiplicities. Polygons define four bins in E_{loss}, used in the analysis.

range from 3.0° to 5.6°, is relevant for this paper. This telescope allowed one to detect and identify, with a low-energy threshold, not only massive products but any products with atomic numbers $1 \leq Z \leq 54$.

Figure 1 presents a two-dimensional contour diagram of the joint distribution of neutron and charged-particle multiplicities from the present reaction, used in this analysis to classify events according to the degree of energy dissipation or impact parameter. The four polygons, superimposed on this plot and labeled 1–4, define four bins with average energy dissipation $\langle E_{loss} \rangle$ of ≈0.1, ≈0.3, ≈0.8, and 1.0 GeV, respectively. The above estimates for $\langle E_{loss} \rangle$, obtained based on series of statistical-model calculations using the code EVAP [30], are consistent with the observed average projectilelike fragment (PLF) velocities. The listed values of average impact parameters were estimated using the above values of $\langle E_{loss} \rangle$ in conjunction with classical trajectory calculations. The latter calculations were performed using the computer code CLAT [31], based on a stochastic nucleon exchange model [32].

Experimental results, representative of IMF production in the reaction studied, are displayed in Figs. 2 and 3. Figure 2 shows a selection of two-dimensional Galilean-invariant velocity distributions for protons, α particles, Li ions, and IMF's ($6 \leq Z \leq 8$) observed in coincidence with PLF's in the most dissipative ^{209}Bi + ^{136} Xe reaction events (bin 4 in Fig. 1). The parallel and perpendicular velocity components, on the abscissa and ordinate of the plot, are defined with respect to the PLF velocity vector in

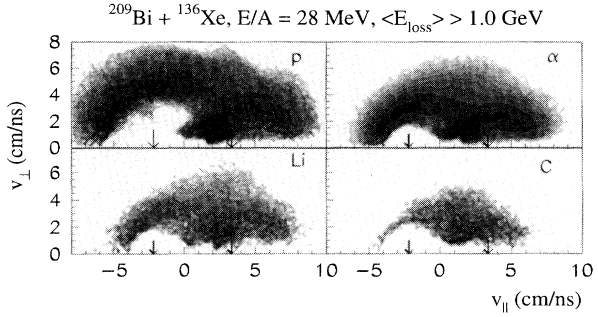

FIG. 2. Logarithmic contour plots of Galilean-invariant emission patterns of LCP's and IMF's, coincident with PLF's, from highly dissipative ($\langle E_{loss} \rangle$1 GeV) ^{209}Bi + ^{136} Xe collisions. Arrows indicate theoretical source velocities.

the center-of-mass system. In Fig. 2, a marked difference is seen between the emission patterns of IMF's, on the one hand, and of protons and α particles (LCP), on the other hand. The yield of LCP's is essentially exhausted by two semicircular "Coulomb" ridges, expected from sequential statistical emission from two moving massive sources, the projectilelike and targetlike fragments. In contrast, a significant portion of the IMF yield is found in an intermediate-velocity component, clearly incompatible with a two-source emission scenario. As seen from Fig. 3, in peripheral collisions (bin 2 in Fig. 1), the latter intermediate-velocity component accounts for most of the IMF yield. The IMF emission patterns of Fig. 3 are consistent with an emission scenario in which IMF's receive, on the average, no significant net Coulomb boost from the rest of the system. Such a scenario would be realized if IMF's were produced dynamically in the interface region between the two hot fragments seen to

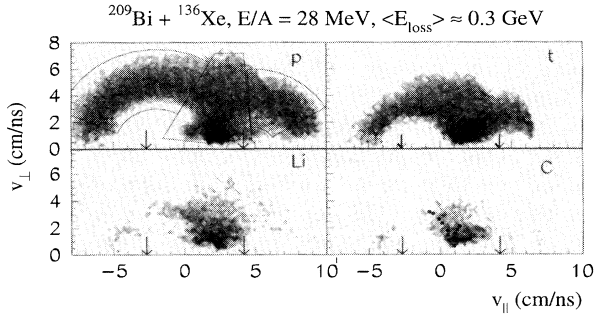

FIG. 3. Logarithmic contour plots of Galilean-invariant emission patterns of LCP's and IMF's, coincident with PLF's, from the peripheral ($\langle E_{loss} \rangle \approx 0.3$ GeV, $b \approx 12.4$ fm) ^{209}Bi + ^{136} Xe collisions. Solid dots in the bottom right panel represent results of relativistic three-body Coulomb-trajectory calculations. The three contour lines in the top left panel illustrate domains used to extract contributions from TLF (left), PLF (right), and neck-zone (NZ) (middle) sources. Arrows indicate theoretical source velocities.

evaporate LCP's (circular Coulomb ridges) at a later stage. In Fig. 2, a pronounced bias towards backward emission, with respect to the PLF velocity, is discernible, the origin of which is not yet clear.

An earlier analysis of the massive-fragment phenomenology of the present reaction has clearly shown [27,28] that the underlying dynamics of peripheral collisions is very similar to that known from studies at lower bombarding energies [33] and that it involves dissipative orbiting or, perhaps, rainbow scattering phenomena. At these lower energies, comparable to the Coulomb barrier, an adiabatic neck is believed to be formed transiently between the reaction partners. One may envision that also at intermediate bombarding energies a necklike zone is formed, which is now, however, unable to adjust adiabatically to the rapidly evolving geometry of the system of two massive fragments. In the present paper, this zone is referred to as the *neck zone,* to distinguish it both from the adiabatic neck considered in the low-energy damped reaction scenario and from the hot participant zone considered in the participant-spectator model for high-energy collisions. Eventually, when the fragments separate, this neck zone is forced to rupture or fragment, giving rise to IMF's.

To verify the compatibility of the IMF emission patterns, displayed in Fig. 3, with the above dynamical production scenario, a series of relativistic three-body Coulomb trajectory calculations were performed, in which IMF's were assumed to be released, with low transversal velocities, from the space between the two massive reaction partners. In these calculations, different scission configurations of three touching charged spheres representing PLF, TLF, and IMF, were assumed, with the sphere representing the IMF placed between those representing PLF and TLF. The scissioning ternary system was assumed to have an angular momentum consistent with the observed degree of kinetic-energy damping, as suggested by classical trajectory calculations (CLAT [31]). In different calculations, the IMF's were allowed to rotate about the center of mass of the system with different angular velocities. The direct results of these calculations were then submitted to a software filter accounting for the geometrical acceptance of the Dwarf Ball/Wall detector array, in order to allow one to perform a meaningful comparison with experimental results. In Fig. 3, results of the above calculations for different ternary scission configurations are shown for neck-zone carbon fragments (solid circles in the right bottom panel). They are seen to agree reasonably well with the experimental carbon emission pattern, thus confirming the viability of the above hypothetical dynamical IMF production scenario.

To obtain quantitative estimates for the relative significance of the two emission scenarios, the observed yields of LCP's and IMF's were decomposed according to the emission sources. Yields attributed to sequential emission from PLF and TLF sources were obtained by extrapolating the respective yields observed in the portions of the invariant velocity distributions (Coulomb ridges) believed to be populated exclusively by either of these two sources (outer contours in the top left panel of Fig. 3). In this extrapolation, it was assumed that these two sources emit particles isotropically. The yield due to dynamical emission from the neck zone was determined by subtracting from the observed yield of intermediate-velocity products (middle contours in the top left panel of Fig. 3) the extrapolated PLF and TLF contributions. Some representative results of such an analysis for peripheral collisions (average kinetic-energy loss $\langle E_{\mathrm{loss}} \rangle \approx 0.3$ GeV are presented in Table I. Uncertainties of the nonzero partial multiplicities listed in this table are assessed at approximately 20%, based on series of decompositions carried out with differently chosen domain contours. As seen from this table, the relative weight of the neck-zone IMF's first increases systematically with the IMF size and then saturates at about 80% of the total multiplicity. The summed multiplicity of approximately 0.24 for IMF's with $3 \leq Z_{\mathrm{IMF}} \leq 8$, originating from the neck zone is quite high as compared to values of 0.001–0.002 typical for low-energy ternary fission α particles. On the other hand, the present study indicates a significant prevalence of tritons over protons as is the case in thermal-neutron-induced ternary fission [34]. This effect is consistent with the relative neutron richness of the nuclear surface forming the neck zone. Table I shows also a significant in-plane versus out-of-plane anisotropy of the IMF yield found in the portion of the velocity distribution associated with the neck zone (domains demarcated by the middle contours in the top left panel of Fig. 3). Such an anisotropy is intuitively consistent with a dynamical emission scenario.

No present theoretical formalism is capable of describing the observed phenomenon quantitatively; however, some insight into the possible multiple neck rupture phenomenon may be sought through Boltzmann-Uehling-Uhlenbeck (BUU) calculations. Sobotka studied, specifically for the present system, the dependence of the neck fragment formation in BUU calculations on the assumed form of the equation of state (EOS) and found [35] that only the "soft" EOS ($K \approx 200$ MeV) would lead to neck fragment formation, and only for impact parameters of about 7 to 8 fm. The inclusion of isospin terms in the interaction potential in these calculations resulted in neck fragments being released in more peripheral collisions, such as discussed in the present paper (impact parameter $b \approx 12.4$ fm, see Fig. 1). Based on general considerations, independent of the BUU approach, one would expect a soft EOS to facilitate multiple neck rupture and to enhance IMF production.

In conclusion, the emission pattern of IMF's from peripheral ^{209}Bi $+^{136}$ Xe collisions at $E_{\mathrm{lab}}/A = 28$ MeV appears indicative of nonequilibrium processes and consistent with a scenario in which IMF's are products of the

TABLE I. Characterization of LCP and IMF yields from the peripheral ($\langle E_{\rm loss}\rangle \approx 0.3$ GeV) ^{209}Bi $+^{136}$ Xe reactions at $E_{\rm lab}/A = 28$ MeV in terms of partial multiplicities associated with TLF, PLF, and NZ sources, and in terms of in-plane versus out-of-plane anisotropy of intermediate-velocity fragment yield ($0°/90°_{\rm NZ}$).

	p	d	t	α	Li	Be	B	C	$6 \le Z \le 8$
$\langle m_{\rm TLF}\rangle$	0.35	0.16	0.15	0.48	0.02	0.01	0.01	0.01	0.02
$\langle m_{\rm PLF}\rangle$	0.28	0.08	0.07	0.28	0.01	0.01	0.00	0.00	0.01
$\langle m_{\rm NZ}\rangle$	0.02	0.02	0.08	0.33	0.06	0.04	0.04	0.03	0.10
% in NZ	4	9	26	30	68	82	83	81	82
$0°/90°_{\rm NZ}$	1.1	1.6	1.6	1.8	2.1	2.5	2.4	2.3	2.4

decoupling of the neck zone from both massive fragments. The likelihood of this kind of process is found surprisingly high, as expressed in the average multiplicity of approximately 0.24 for neck-zone IMF's with $3 \le Z_{\rm IMF} \le 8$. One may expect the latter likelihood to reflect the macroscopic properties and behavior of nuclear matter in the neck zone and, hence, the present work suggests new exciting opportunities to study these properties under controlled experimental conditions. Clearly, more stringent theoretical modeling and more systematic experimental investigations are necessary, in order to establish the pertinent features of the different IMF production mechanisms.

This work was supported by U.S. Department of Energy Grants No. DE-FG02-88ER40414 (University of Rochester), No. DE-FG02-87ER403160, and No. DE-FG02-88ER40406 (Washington University), and by National Science Foundation Grant No. PHY-89-13815 (NSCL).

*On leave from CRN Strasbourg, BP 20 CRO, F-67037 Strasbourg, France.
†Present address: GANIL, BP 5027, F-14021 Caen, France.
‡On leave from Instituto de Fisica da UFRJ, Rio de Janeiro, Brazil.
§Present address: Oak Ridge National Laboratory, Oak Ridge, TN 37830.

[1] C. K. Gelbke and D. H. Boal, Prog. Part. Nucl. Phys. **19**, 33 (1987), and references therein.
[2] B. Borderie *et al.*, Ann. Phys. (Paris) **15**, 287 (1990), and references therein.
[3] D. R. Bowman *et al.*, Phys. Rev. C **46**, 1834 (1992).
[4] L. G. Moretto and G. J. Wozniak, Annu. Rev. Nucl. Part. Sci. **43**, 379 (1993), and references therein.
[5] W. A. Friedman, Phys. Rev. Lett. **60**, 2125 (1988).
[6] W. A. Friedman, Phys. Rev. C **42**, 667 (1990).
[7] A. Sokolov *et al.*, Nucl. Phys. **A562**, 273 (1993).
[8] J. L. Wile *et al.*, Phys. Lett. B **264**, 26 (1991).
[9] R. Vandenbosch and J. R. Huizenga, in *Nuclear Fission* (Academic Press, New York, 1973), and references therein.
[10] U. Brosa *et al.*, Z. Phys. A **310**, 177 (1983).
[11] U. Brosa *et al.* Phys. Rep. **197**, 167 (1990).
[12] J. P. Theobald *et al.*, Nucl. Phys. **A502**, 361c (1989), and references therein.
[13] W. W. Wilcke *et al.*, Phys. Rev. Lett. **51**, 99 (1983).
[14] J. P. Kosky *et al.*, Phys. Lett. **133B**, 153 (1983).
[15] R. Lacey *et al.*, Phys. Rev. C **37**, 2540 (1988).
[16] G. Casini *et al.*, Phys. Rev. Lett. **71**, 2567 (1993).
[17] A. A. Stefanini *et al.*, Z. Phys. A **351**, 167 (1995).
[18] D. E. Fields *et al.*, Phys. Rev. Lett. **69**, 3713 (1992).
[19] P. R. Brazier-Smith *et al.*, Proc. R. Soc. London A **326**, 393 (1972).
[20] A. Menchaca-Rocha *et al.*, Phys. Rev. E **47**, 1433 (1993).
[21] L. G. Moretto *et al.*, Phys. Rev. Lett. **69**, 1884 (1992).
[22] C. P. Montoya *et al.*, Phys. Rev. Lett. **73**, 3070 (1994).
[23] B. Lott *et al.*, in *Proceedings of the 9th Winter Workshop on Nuclear Dynamics, Key West, 1993* (World Scientific, Singapore, New Jersey, London, Hong Kong, 1993), p. 159.
[24] W. U. Schröder, in *Proceedings of the International School-Seminar on Heavy Ion Physics, Dubna, 1993* (World Scientific, Singapore, 1994), p. 166.
[25] J. Tõke *et al.*, Nucl. Phys. **A583**, 519 (1995).
[26] B. Lott *et al.*, Phys. Rev. Lett. **68**, 3141 (1992).
[27] S. P. Baldwin *et al.*, in *Proceedings of the 9th Winter Workshop on Nuclear Dynamics, Key West, 1993* (World Scientific, Singapore, New Jersey, London, Hong Kong, 1993), p. 36.
[28] S. P. Baldwin *et al.*, Phys. Rev. Lett. **74**, 1299 (1995).
[29] D. W. Stracener *et al.*, Nucl. Instrum. Methods Phys. Res., Sect. A **294**, 485 (1990).
[30] N. Nicolis *et al.*, computer code EVAP (unpublished); evolved from code PACE by A. Gavron, Phys. Rev. C **21**, 230 (1980).
[31] W. U. Schröder *et al.*, Nucl. Sci. Res. Conf. Ser. **11**, 255 (1987).
[32] J. Randrup, Nucl. Phys. **A307**, 319 (1978); **A327**, 490 (1979); **A383**, 468 (1982).
[33] W. U. Schröder and J. R. Huizenga, in *Treatise in Heavy-Ion Science,* edited by D. A. Bromley (Plenum Press, New York, London, 1984), Vol. 2, p. 113, and references therein.
[34] C. Wagemans, in *The Nuclear Fission Process,* edited by C. Wagemans (CRC Press, Boca Raton, 1991), p. 545.
[35] L. G. Sobotka, Phys. Rev. C **50**, R1272 (1994).

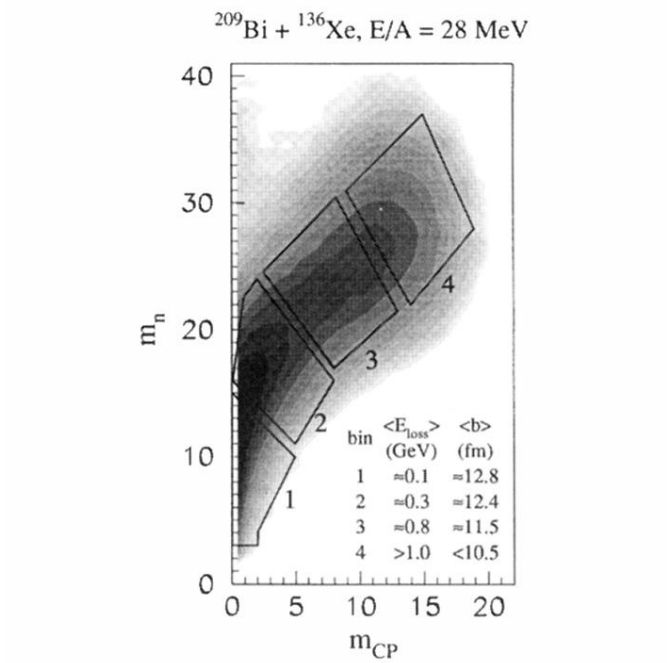

FIG. 1. Logarithmic contour plot of the joint distribution of neutron and charged-particle multiplicities. Polygons define four bins in E_{loss}, used in the analysis.

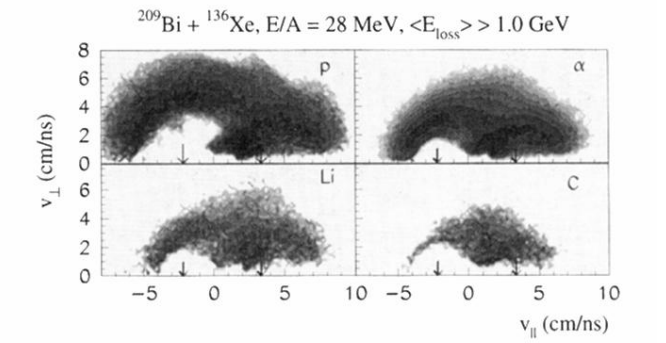

FIG. 2. Logarithmic contour plots of Galilean-invariant emission patterns of LCP's and IMF's, coincident with PLF's, from highly dissipative ($\langle E_{loss}\rangle$1 GeV) ^{209}Bi + ^{136} Xe collisions. Arrows indicate theoretical source velocities.

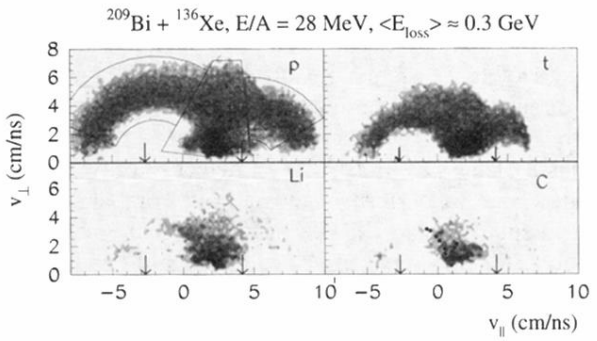

FIG. 3. Logarithmic contour plots of Galilean-invariant emission patterns of LCP's and IMF's, coincident with PLF's, from the peripheral ($\langle E_{\rm loss}\rangle \approx 0.3$ GeV, $b \approx 12.4$ fm) ^{209}Bi + ^{136}Xe collisions. Solid dots in the bottom right panel represent results of relativistic three-body Coulomb-trajectory calculations. The three contour lines in the top left panel illustrate domains used to extract contributions from TLF (left), PLF (right), and neck-zone (NZ) (middle) sources. Arrows indicate theoretical source velocities.